Chemical Research in Toxicology

pubs.acs.org/crt

Article

Sterile Inflammation in Mouse Lung Driven by Lipid Mediator Pathways Following MWCNT Exposure

Qiang Ma,* Ryan F. LeBouf, Chengetayi Cornelius Rimayi, Chol Seung Lim, Desta Fekedulegn, Ju-Hyeong Park, and Dale W. Porter

Cite This: *Chem. Res. Toxicol.* 2026, 39, 189−203

Read Online

ACCESS | Metrics & More | Article Recommendations | Supporting Information

ABSTRACT: Exposure to respirable particles such as multiwalled carbon nanotubes (MWCNTs) can provoke acute lung inflammation and tissue injury, potentially progressing to chronic disease. Lipid mediators (LMs), including proinflammatory and pro-resolving species, play a critical role in regulating this process. This study investigated LM biosynthesis in acute lung inflammation induced by fibrogenic MWCNTs. Adult C57BL/6J mice were exposed to MWCNTs (Mitsui-7; 1860.4 μg/kg) via oropharyngeal aspiration. Lung tissues collected 24 h postexposure exhibited neutrophil infiltration, elevated inflammatory cytokines, and tissue damage. Enzymes involved in prostanoid synthesis—phospholipase A2, cyclooxygenase-2, and prostaglandin E synthase—were significantly upregulated. Lipidomic profiling was performed by using C18 spin column enrichment and UPLC-MS/MS. MWCNT exposure significantly increased the levels of prostanoids (PGE2, PGD2, PGF2α, thromboxane B2) and hydroxyeicosatetraenoic acids (5-, 12-, 15-HETE). Elevated levels of protectin DX, 14(*S*)-, and 17-HDHA derived from docosahexaenoic acid, and 12-, 15-, and 18-HEPE derived from eicosapentaenoic acid were also observed. In vitro, MWCNTs induced intracellular lipid accumulation in macrophages. These findings reveal rapid activation of LM biosynthetic pathways, particularly those producing proinflammatory prostanoids, in mouse lungs following nanoparticle exposure. The study underscored the utility of lipidomic profiling for mechanistic insights into nanoparticle-induced sterile inflammation and toxicity in limited tissue samples.

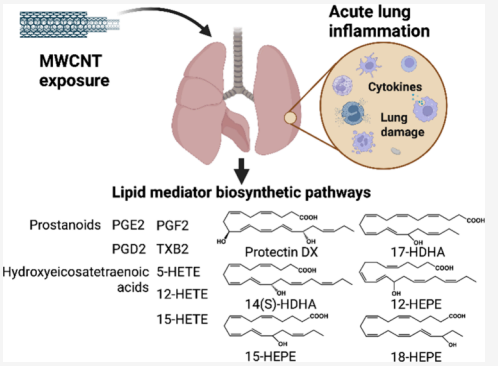

INTRODUCTION

Carbon nanotubes (CNTs) are carbon allotropes composed of hexagonally arranged atoms formed through sp^2 hybridization, creating graphene-like lattices rolled into concentric cylinders.[1] CNTs possess unique anisotropic properties that have attracted significant interest for technological, industrial, and commercial applications.[2] They exhibit high elastic modulus and tensile strength, metallic or semiconducting electrical properties depending on lattice chirality, and exceptional thermal conductivity—up to 3500 W/mK. Additionally, CNTs have a high surface-to-volume ratio and can be chemically functionalized. CNTs are incorporated into a wide range of products, including composite materials, batteries, supercapacitors, microelectronics, textiles, coatings, films, and solar cells.[3] Recent applications have expanded into energy storage and conversion, wearable sensors, environmental remediation (including CO_2 reduction), and biomedical fields such as drug delivery, biosensing, and tissue engineering.[4] Multiwalled CNTs (MWCNTs) have been more commonly used in applications due to their lower production cost.

Despite their promising applications, certain properties of CNTs raise health and environmental concerns.[5] Their lightweight and airborne nature makes them difficult to contain in open environments and easy to inhale. The strong sp^2 carbon−carbon bonds render CNTs resistant to biological and environmental degradation, making them persistent contaminants and long-lasting foreign bodies in the human body. Toxicological studies have shown that pulmonary exposure to certain CNTs in laboratory animals can lead to a range of acute and chronic lesions in the airways, alveolar space, and pleura—including inflammation, fibrosis, lung cancer, and mesothelioma-like malignancy.[6−8] Although human exposure studies are still in early stages, these findings raise concerns about potential health risks like those caused by inhalation of mineral particles and fibers, such as silicosis and mesothelioma.[9,10] Workplace exposure to CNTs and CNT-containing materials is a particular concern for occupational safety and health at the workplace.[11]

Received: November 2, 2025
Revised: December 1, 2025
Accepted: December 3, 2025
Published: December 15, 2025

Inflammation is a common and often dominant response to CNT exposure in the lungs. Under normal physiological conditions, inflammation serves as a protective mechanism against inhaled particles and nanoparticles, aiding in particle clearance and tissue repair.[12,13] However, persistent exposure and unresolved inflammation can lead to chronic conditions, such as fibrosis and cancer in the lungs and pleura. In such cases, inflammation acts as a precursor to chronic disease outcomes.[9] At the tissue level, inflammation induced by CNTs reflects an innate immune response to foreign materials, manifested as sterile inflammation. This process begins with the rapid infiltration of neutrophils, the release of inflammatory cytokines, and the subsequent tissue damage. Over time, the response transitions to a macrophage-dominated phase, accompanied by fibroproliferative activity near the site of particle deposition.[14] This shift highlights the dual role of inflammation in either facilitating tissue repair or contributing to the chronic progression of lesions, ultimately leading to the formation of granulomas, fibrosis, and scar-associated cancers.[9,13,15,16]

The regulation of inflammation and its resolution involve complex immune responses and mediators, with increasing attention given to lipid mediators (LMs), including inflammatory LMs (ILMs) and specialized pro-resolving mediators (SPMs).[17,18] During acute inflammation, arachidonic acid (AA) released from membrane phospholipids is enzymatically converted into prostaglandins (PGs), thromboxane (TX), and leukotrienes (LTs) via cyclooxygenases (COXs) and arachidonate lipoxygenases (ALOXs).[17,19] These ILMs play key roles in initiating and amplifying inflammation, making their synthesis and signaling pathways major targets of anti-inflammatory drugs.[20] In contrast, SPMs are produced later to promote resolution and tissue repair.[21] SPMs include lipoxins (LXs) from the AA pathway, resolvin Es (RvEs) from the eicosapentaenoic acid (EPA) pathway, and resolvin Ds (RvDs), protectins, and maresins (MaRs) from the docosahexaenoic acid (DHA) pathway.[18]

Analyzing bioactive LMs in inflamed tissues is challenging due to their shared precursors—AA, DHA, and EPA—which result in structural similarities, including isobars and optical isomers. Additionally, each LM family includes numerous intermediate, active, and inactive metabolites. Many bioactive LMs are present in tissues at picogram to nanogram levels, often with short half-lives and specific temporal profiles.[22] While methods for LM quantification exist, they are often costly and require large tissue quantities. To address these limitations, high-performance liquid chromatography coupled with tandem mass spectrometry (HPLC-MS/MS), following solid-phase lipid extraction, has been developed. When combined with chemically synthesized LM standards, this approach enables systematic identification and quantification of bioactive LMs from AA, EPA, and DHA pathways.[23] However, sensitive and quantitative methods for profiling LMs in toxicant-induced sterile inflammation in the lung—where tissue quantity is limited and multiparameter analysis is needed—remain underdeveloped.

We previously reported that exposure to fibrogenic MWCNTs stimulates early production of proinflammatory LMs such as PGE_2 and LTB_4 in mouse lungs and the broncoalveolar lavage fluid (BALF), followed by later production of SPMs including RvDs and lipoxins.[16] Other studies have shown COX-2 induction in cultured macrophages[24] and its role in allergen-induced airway remodeling by MWCNTs.[25] These findings suggest that ILMs and SPMs play key roles in regulating the initiation and resolution of MWCNT-induced lung inflammation. However, previous studies have focused on a small number of LMs or enzymes due to limitations of the analytical methods used, restricting their ability to fully characterize the broader pulmonary response to nanoparticle exposure.

In this study, we developed a UPLC-MS/MS procedure and performed lipidomic analysis to profile ILMs and SPMs during acute inflammation in mouse lungs exposed to fibrogenic MWCNTs. To facilitate this analysis, we utilized a C18 spin column-based solid-phase extraction method to enable rapid and efficient enrichment of LMs from small quantities of lung tissue. UPLC-MS/MS was performed using the Waters ACQUITY Xevo TQ-XS system equipped with an ACQUITY HSS T3 column. Our lipidomic and molecular analysis revealed a robust activation of prostaglandin synthesis, characterized by significantly elevated levels of prostaglandins and other prostanoids, alongside marked induction of phospholipase A2 (PLA2), cyclooxygenase-2 (COX-2), and prostaglandin E synthase (PGES). These findings demonstrate the effectiveness of UPLC-MS/MS-based lipidomic analysis for investigating inflammation and nanotoxicity in mouse lungs, particularly when limited tissue samples are available for comprehensive toxicological and mechanistic studies. The results underscore the pivotal role of prostaglandins in initiating and propagating acute sterile inflammation in the lung following MWCNT exposure.

MATERIALS AND METHODS

Chemicals and Reagents. Methanol (>99.9%, LCMS grade), acetonitrile (>99.9%, LCMS grade), acetic acid (≥99.7%, LCMS grade), and ammonium acetate used in the mobile phase buffer (≥99.0%, LCMS grade) were purchased from Fisher Scientific (Waltham, MA, USA). Analytical standards with purities ≥98% were purchased from Cayman Chemicals (Ann Arbor, MI, USA). A C18 spin column (BioPureSPN Midi PROTO 300 C18, 17−170 μg, P/N HEM S18V) used for tissue lipid extraction were obtained from The Nest Group (Ipswich, MA, USA).

MWCNT Preparation. The MWCNTs used in this study were obtained from Mitsui & Company (Mitsui-7, XNRI 1, lot # 0507 2001K28, Tokyo, Japan) and prepared as described previously.[6,16] A dispersion medium (DM; 0.9% saline supplemented with 0.6 mg/mL mouse serum albumin and 0.01 mg/mL 1,2-dipalmitoyl-*sn-glycero*-3-phosphocholine) was used to prepare suspensions of MWCNTs following a two-step dispersion procedure. DM was used as a vehicle for nanotubes in animal studies. The chemicals used in DM were from Millipore Sigma (Burlington, MA, USA). The length distribution of the MWCNTs is log-normal with a mean of 4.46 μm (95% confidence interval of 4.08−4.88 μm). The width distribution is normally distributed with a mean of 58.5 nm (95% confidence interval of 56.0−61.0 nm). The average surface area is 26 m^2/g as shown by nitrogen adsorption−desorption. Trace elements were low with 0.78% for all metals and 0.32% for iron.[6] The level of lipopolysaccharides (LPSs) in the MWCNTs was determined to be <0.1 EU/mL (<0.01 mg/mL) using the Pierce LAL chromogenic endotoxin quantification kit (Thermo Fisher, Pittsburgh, PA, USA).

Animal Treatment. Eight-week-old male mice (C57BL/6J) were purchased from Jackson Laboratories (Bar Harbor, ME, USA). Mice were maintained in an accredited, specific pathogen-free, and environmentally controlled facility at the National Institute for Occupational Safety and Health. All animals received humane care, and all experiments involving animals were performed following the protocols evaluated and approved by the Institutional Animal Care and Use Committee, National Institute for Occupational Safety and Health at the Morgantown Facility (approval number: 23-004). Mice

https://doi.org/10.1021/acs.chemrestox.5c00470
Chem. Res. Toxicol. 2026, 39, 189−203

were treated with a single dose of DM or MWCNTs (1860.4 μg/kg body weight) at a volume of 50 μL per mouse; the MWCNTs at this dose have been shown to induce significant inflammatory responses in mouse lungs.[6,16] Administration of the agent was by pharyngeal aspiration as described previously.[6,7] Mice were euthanized with an intraperitoneal injection of a sodium pentobarbital euthanasia solution (100−300 mg/kg body weight; Zoetis, Florham Park, NJ, USA), followed by exsanguination once the mouse was unresponsive to a toe pinch. Lung tissue was collected, minced, and frozen in liquid nitrogen and was stored at −80 °C for lipidomic and protein analyses.

Transmission Electron Microscopy (TEM). MWCNTs were imaged by using TEM for their morphology and size characteristics. Stock samples were prepared above and were diluted in double distilled water to 1:300. One drop of the samples was placed onto a Formvar-coated 200 mesh copper grid and allowed to dry overnight. Images were taken using a JEOL 1400 TEM instrument (Tokyo, Japan) at 80 kV.

Immunohistochemistry. The mouse's left lung was formalin-fixed, paraffin-embedded, and sectioned to 5 μm following standard procedures. The sections were deparaffinized with three washes of xylene (5 min each), two washes of 95% ethanol (10 min each), and one wash of 70% ethanol (5 min). To unmask antigens, the sections were heated to boil in a 10 mM sodium citrate buffer, pH 6.0, and maintained at a subboiling temperature for 10 min in a microwave oven. The slides were incubated with BLOXALL endogenous peroxidase and alkaline phosphatase blocking solution (Vector Laboratories, Burlingame, CA, USA) for 10 min to block the endogenous peroxidase activities. Immunohistochemistry was performed with the ImmPRESS polymer detection system (Vector Laboratories) using ImmPACT NovaRED as the peroxidase substrate (red). Nuclei were counterstained with Hematoxylin OS (blue-violet, Vector Laboratories). The primary antibodies used were anti-Mac-2 (Cedarlane, Burlington, Ontario, Canada) and antineutrophil (Abcam, Cambridge, MA, USA) antibodies. Images were photographed using Olympus Provis AX-70 (Olympus, Center Valley, PA, USA). Stained cells were quantified by counting five images at 40× magnification per section. Lung sections from four mice in each group were examined.

Mouse Bronchoalveolar Lavage (BAL). Mice were euthanized as described above. A tracheal cannula was inserted into the trachea, and BAL was performed through the cannula using ice cold Ca^{2+}- and Mg^{2+}-free phosphate-buffered saline (PBS), pH7.4, as described in detail previously.[16] BALF samples were collected and stored at −80 °C until use.

UPLC-MS/MS Analytical Method. *Liquid Chromatography.* A liquid chromatography-tandem quadrupole mass spectrometer (Waters ACQUITY Xevo TQ-XS UPLC-MS, Waters, Milford, MA, USA) was utilized for lipidomic analysis. The Acquity Premier UPLC system operates with an ACQUITY Premier column (ACQUITY Premier HSS T3 column with a VanGuard FIT, 1.8 μm, 2.1 mm × 100 mm, product number 186009471, Waters) using a 10 μL injection volume. The column and sample tray temperatures were maintained at 50 and 4 °C, respectively, throughout chromatographic runs. The mobile phase gradient consisted of solvent A (95% Milli-Q ultrapure water, 5% methanol, and 0.01% acetic acid with 10 mM ammonium acetate) and solvent B (95% methanol, 5% Milli-Q ultrapure water, and 0.01% acetic acid with 10 mM ammonium acetate). The ultrapure water was dispensed through a Millipore LC pak polisher cartridge (Millipore Sigma). The mobile phase was set at a flow rate of 200 μL/min and initialized at 100% solvent A and 0% solvent B to 30% solvent A and 70% solvent B from 0 to 17 min. Solvent B was gradually increased to 85% from 17 to 20 min and to 100% at 25 min with a hold for 2 min before reducing to 0% from 27 min to 28, followed by an additional hold of 2.5 min. The total runtime was 30.5 min for one cycle of run.

MS Parameters and Transitions. The tandem quadrupole mass spectrometer (Waters Xevo TQ-XS) was operated with an electrospray ionization (ESI) source in negative-ionization mode for the analysis of target analytes. The instrument was operated with an ESI capillary voltage of 1.5 kV and with a source temperature and desolvation temperature of 150 and 250 °C, respectively. Laboratory-generated high-purity nitrogen (Peak Scientific Instruments, Westford, MA, USA) was used with desolvation and cone gas flow rates of 600 and 150 L/hour, respectively. The collision cell entrance potential was set to 30 V and the exit potential to 30 V. The system was run in the multiple reaction monitoring (MRM) mode, with 4 to 5 optimized transitions for each compound except for 12-hydroxyeicosapentaenoic acid (12-HEPE), where 2 reliable transitions were optimized and used. The cone voltage and collision energy were individually optimized for each compound as shown in Supplemental Table 1.

UPLC-MS/MS Standards and Quantification. Internal standard quantification was performed using TargetLynx and MassLynx V4.2. Briefly, 100 pg/μL internal standards were added to both samples and external standards. Calibration standards for the 36 target LMs were prepared at 2 different calibration ranges to accommodate the different levels of endogenous concentrations of target LMs in samples. The linear calibration range was from 0.66 to 675 pg/μL for LMs except EPA, AA, and DHA, which have a linear calibration range of 0.82 to 13,500 pg/μL. The limit of detection (LOD) and limit of quantification (LOQ) were calculated at 3× and 10× the signal-to-noise ratio, respectively.

Sample Preparation. Mouse lung tissue was collected and homogenized in 375 μL of ice cold methanol (#A456-500, LC/MS grade, Fisher Scientific) spiked with 25 μL of the internal standard mixture with a Dounce homogenizer. The homogenates were incubated at −20 °C for 30 min before centrifugation at 751*g* for 10 min to obtain supernatants. The supernatant was then acidified to pH 3.5 prior to solid-phase extraction.

C18 Spin Column Solid-Phase Extraction. A C18 spin column-based method was developed to enable fast and efficient solid-phase extraction of ILMs and SPMs from small quantity samples, such as mouse lung tissue. Sample homogenate supernatants described above were evaporated using a TurboVap (Zymark, Hopkinton, USA) under a gentle stream of nitrogen followed by reconstitution in 250 μL of Milli-Q water:methanol, 80:20 (v/v) and mixing by vortex for 15 s. Each sample extract was added to a preconditioned C18 spin tube followed by pulse spinning up to 1500 RCF and removal of the flowthrough. The C18 spin tubes were washed with 2 volumes of 250 μL of Milli-Q water:methanol, 80:20 (v/v), with the spin tube rotated 180° and the flowthrough discarded after each wash. SPMs were eluted by adding 250 μL of acetonitrile:Milli-Q water, 80:20 (v/v) on top of the C18 sorbent, and centrifugation by pulse spin past 1500 RCF. The flowthrough was collected in a 1.5 mL centrifuge tube. The collected flowthrough was evaporated to dryness using a TurboVap, with a gentle stream of nitrogen at 47 °C. A volume of 50 μL of LC-MS mobile phase solvent A:B, 1:1, (v/v) was added to each centrifuge tube to reconstitute with the vortex. The solvent was transferred to a vial LC insert for immediate LC-MS/MS analysis together with freshly made calibration standards.

Phospholipase A2 (PLA2) Enzyme Activity. The enzymatic activity of secreted PLA2 (sPLA2) was measured using a sPLA2 assay kit (#765001, Cayman Chemical) according to the manufacturer's instructions. Mouse lung tissue was collected and homogenized in an assay buffer (25 mM Tris-Cl, pH 7.5, 10 mM $CaCl_2$, 100 mM KCl, and 0.3 mM Triton X-100) with a Dounce homogenizer. The reaction mixture for sPLA2 (225 μL) contained 10 μL of tissue sample, 10 μL 5,5′-dithiobis 2-nitrobenzoic (DTNB), 5 μL of assay buffer, and 200 μL of diheptanoyl Thio-PC substrate solution. The same volume of reaction mixture containing 10 μL of DTNB, 15 μL of assay buffer, and 200 μL of substrate solution was used as a negative control. The venom PLA2 supplied with the kit was used as a positive control. Enzyme activity was measured by using a spectrofluorometer (Biotek synergy H1 multimode plate reader, Santa Clara, CA, USA). Changes in absorbance at 414 nm from the reaction product were measured and plotted to obtain the slope of a linear curve. Specific enzyme activity was calculated with an extinction coefficient of DTNB (10.66 mM^{-1} cm^{-1}). Samples of each treatment group were assayed in duplicates.

https://doi.org/10.1021/acs.chemrestox.5c00470
Chem. Res. Toxicol. 2026, 39, 189−203

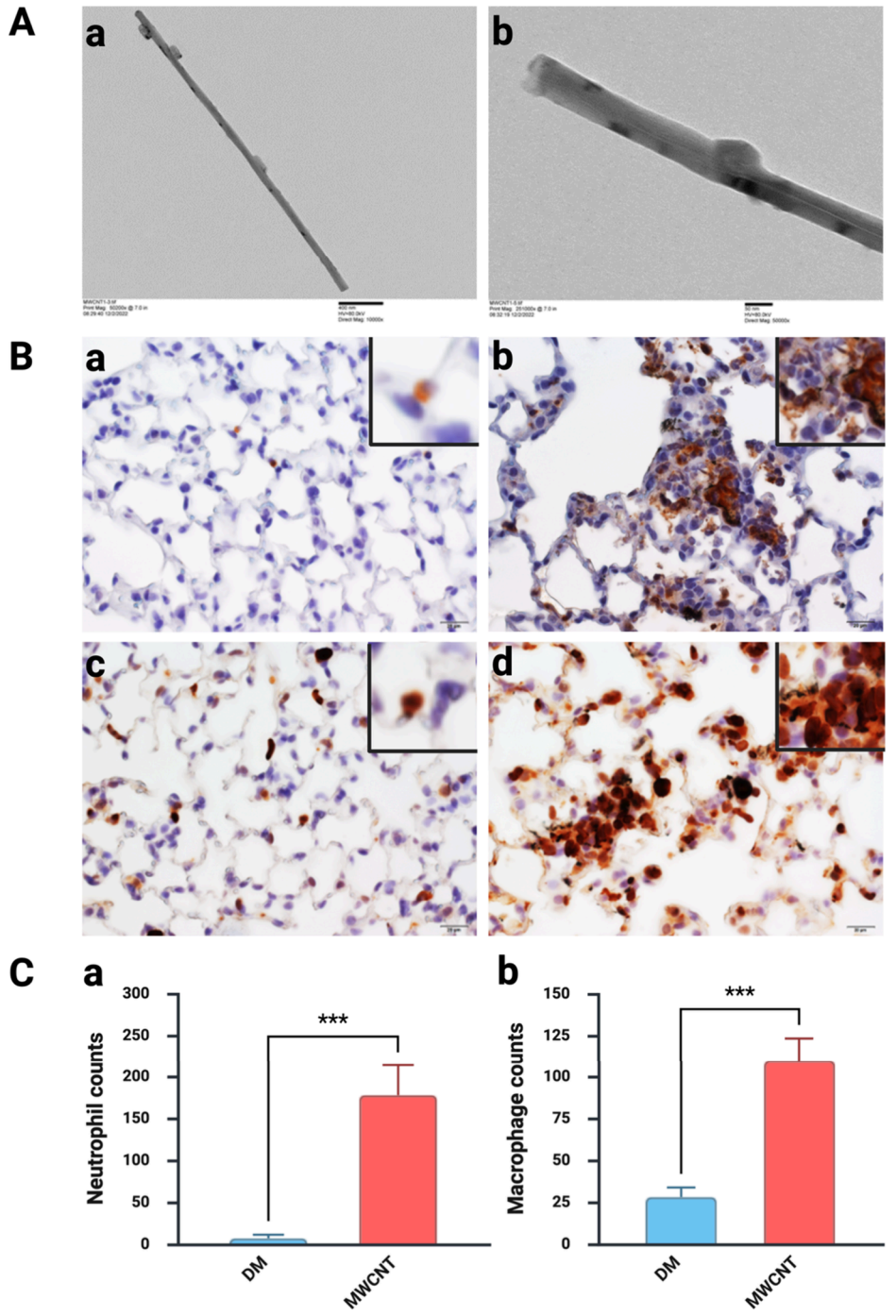

Figure 1. Acute inflammation in mouse lungs exposed to MWCNTs. Adult C57BL/6J mice were exposed to DM (vehicle) or MWCNTs (40 μg/21.5 g of body weight) by oral pharyngeal aspiration. Lung tissue was collected at 24 h postexposure. (A) Morphology of MWCNTs under TEM. Images were taken at a magnification of 10,000× (a) or 50,000× (b). (B) Immunohistochemistry showing neutrophils or macrophages in DM- (a and c) or MWCNT-exposed (b and d) lungs, respectively. MWCNTs induced prominent infiltration and clustering of Ly-6G- and Ly-6C-positive neutrophils in the vicinity of MWCNT deposits (b) and inflammatory foci with clusters of Mac2-positive macrophages engulfing MWCNTs (d). Scale bars were set at 20 μm. (C) Quantification of neutrophils (a) and macrophages (b) in lungs. Data represent mean ± STDs from 4 mice in each group. ***, $p < 0.001$.

The cytosolic PLA2 (cPLA2) activity was determined by using a cPLA2 assay kit (#765011, Cayman Chemical) following the manufacturer's instructions. Lung tissue was collected and homogenized in an ice cold buffer (50 mM HEPES, pH 7.4, and 1 mM EDTA). The reaction mixture (225 μL) contained 10 μL of sample, 10 μL of 5,5′-dithiobis 2-nitrobenzoic (DTNB), 5 μL of assay buffer, and 200 μL of arahidonoyl thio-PC substrate solution. The same volume of reaction mixture containing 10 μL of DTNB, 15 μL of assay buffer, and 200 μL of substrate was used as a negative control. The venom PLA2 supplied with the kit was used as a positive control. To inhibit sPLA2 or cPLA2, 5 μL of thioetheramide-PC (TEA-PC, sPLA2 inhibitor, Cayman Chemical, item #62750, final concentration of 5 μM) or pyrrophenone (cPLA2 inhibitor, Cayman Chemical, item #13294, final concentration of 10 nM) was added to the reaction mixture, respectively. Enzyme activity was measured and calculated as described for sPLA2.

https://doi.org/10.1021/acs.chemrestox.5c00470
Chem. Res. Toxicol. 2026, 39, 189−203

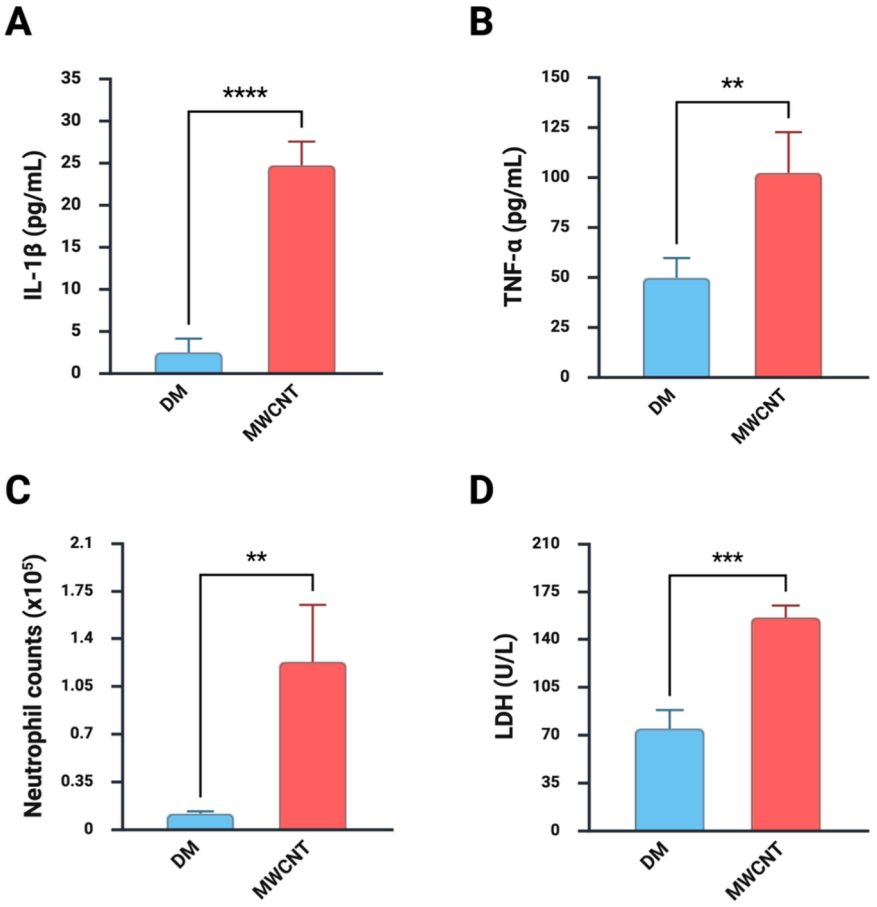

Figure 2. BALF inflammation and toxicity. BALF was prepared from mouse lungs exposed to DM or MWCNTs and examined for inflammatory and toxicity parameters. Inflammatory cytokines IL-1β (A) and TNF-α (B) were quantified by ELISA. Quantification of neutrophils was shown in (C). LDH activity was measured to indicate cellular damage and toxicity (D). Data represents mean ± STDs from 4 mice each group. **, $p < 0.01$; ***, $p < 0.001$; ****, $p < 0.0001$.

COX Enzyme Activity. A COX activity assay kit (#760151, Cayman Chemical) was used to determine the enzyme activity of COX by monitoring the appearance of oxidized *N*,*N*,*N*′,*N*′-tetramethyl-*p*-phenylenediamine (TMPD) by color, following the manufacturer's instructions. Mouse lung samples were collected and prepared as described above. The reaction mixture (210 μL) was composed of 40 μL of a sample, 10 μL of hemin, and 120 μL of the assay buffer. A heat-inactivated sample of the same volume was used in the background reaction, whereas the assay buffer of 40 μL with no sample was used as the negative control. COX standards provided in the kit were used as positive controls. To measure the COX-1 or COX-2 isoform-specific activity, 10 μL of SC-560 (an inhibitor of COX-1) or 10 μL of DuP-697 (an inhibitor of COX-2) supplied with the kit was used. The reagents were mixed and incubated for 5 min at 25 °C, followed by the addition of 20 μL of a colorimetric substrate solution containing TMPD and 20 μL of AA at a final concentration of 2.2 mM. Incubation was continued for 5 min at 25 °C, and the absorbance at 590 nm was measured using the Biotek synergy H1 multimode plate reader. Correction in absorbance was made by subtracting the background value from the corresponding samples and the inhibitor-treated samples. The total COX activity was calculated using the extinction coefficient of TMPD (0.00826 μM^{-1} cm^{-1}). Samples from each treatment were assayed in duplicates. The COX-1- and COX-2-specific activities were calculated by subtracting the COX activity of a sample treated with the COX-1 or the COX-2 specific inhibitor, respectively, from the total COX activity of the corresponding sample without the inhibitor.

Cell Culture and Lipid Stain. J774A.1 murine macrophage cells were purchased from American Type Culture Collection (ATCC, Manassas, VA, USA) and were cultured in Dulbecco's Modified Eagle's Medium (DMEM, Thermo Fisher) with 10% fetal bovine serum (FBS, Thermo Fisher) at 37 °C with 5% CO_2. For cell treatment, MWCNTs were suspended in DMEM with 1% FBS by vortexing and sonication. DMEM with 1% FBS was used as the vehicle control. Cells were grown in a 24-well plate overnight, followed by treatment with vehicle or MWCNTs (2 μg/mL) for 24 h. Cells were then stained with the LipidTox Green neutral lipid stain reagents (Thermo Fisher) for an additional 24 h before fixation with 3.7% formaldehyde. 4',6-Diamidino-2-phenylindole (DAPI, Thermo Fisher) was used to counterstain the nucleus. Images were taken using the Agilent BioTek Cytation 1 Cell Imaging Multi-Mode Reader, model CYT1FAV (Agilent Technologies, Santa Clara, CA, USA), using phase contrast for optical morphology or a DAPI filter for DAPI fluorescence intensity (EX 360/EM 460 nm) and a GFP filter for LipidTox Green fluorescence intensity (EX 495/EM 505 nm). Scale bars were set at 200 μm. Images were taken at the same settings and were analyzed for relative fluorescence intensity (RFU) using the Agilent BioTek Gen5 software (Agilent Technologies). Data represent mean ± SD from 4 separate populations.

Immunoblotting. Lung tissue collected from mice exposed to DM or MWCNT for 1 day was minced and homogenized in a lysis buffer (10 mM Tris, pH 7.4, 1% SDS) containing a 1× proteinase inhibitor cocktail (Thermo Fisher) using a tissue homogenizer (OMNI International, Kennesaw, GA, USA). Tissue extracts were obtained by centrifugation of the tissue homogenate at 15,000*g*, 4 °C for 10 min. Protein concentrations of the extracts were determined using a bicinchoninic acid protein assay kit (Thermo Fisher). Extracts (10–20 μg each) were resolved on a 10 or 12% SDS-PAGE gel. Protein bands were transferred to a nitrocellulose membrane. The membrane was incubated with 5% nonfat dry milk in Tris-buffered

https://doi.org/10.1021/acs.chemrestox.5c00470
Chem. Res. Toxicol. 2026, 39, 189−203

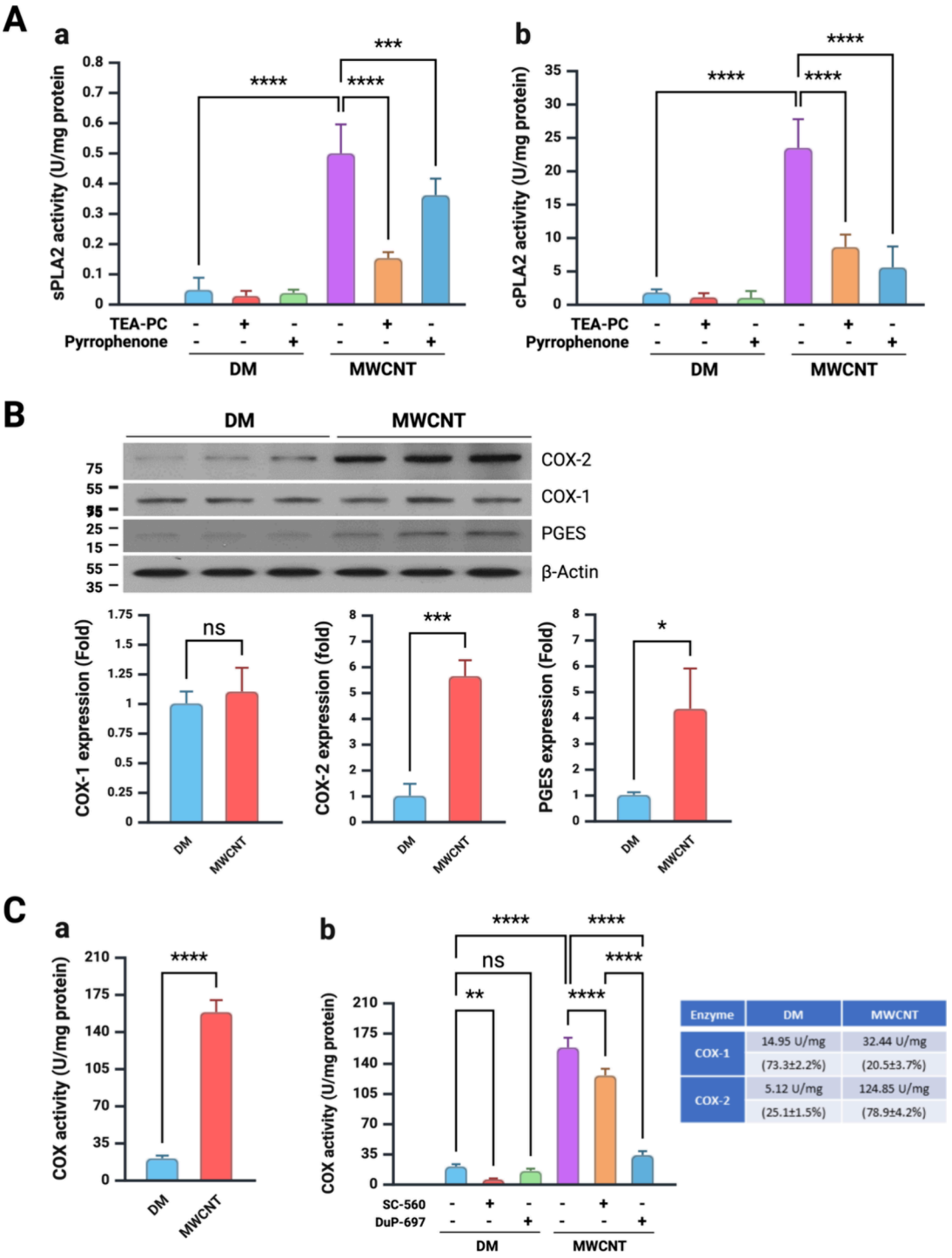

Enzyme	DM	MWCNT
COX-1	14.95 U/mg	32.44 U/mg
	(73.3±2.2%)	(20.5±3.7%)
COX-2	5.12 U/mg	124.85 U/mg
	(25.1±1.5%)	(78.9±4.2%)

Figure 3. Induction of key enzymes for PG synthesis in mouse lungs. Homogenates were prepared from mouse lungs exposed to DM or a single dose of MWCNTs for 24 h. (A) PLA2 activity. PLA2 activities were determined for sPLA2 (a) and cPLA2 (b). TEA-PC, a specific inhibitor of sPLA2, and pyrrophenone, a specific inhibitor of cPLA2, were used to differentiate the activities of sPLA2 and cPLA2. (B) Immunoblotting. Protein levels of COX-1, COX-2, and PGES were determined by immunoblotting. β-Actin was used as a loading control. Quantitation of protein bands was shown in bar figures. Data represents means ± STDs from 3 separate blots. (C) COX activity. Total COX activities in lung homogenates were determined (a). Activities of COX-1 and COX-2 were differentiated by using SC-560, an inhibitor of COX-1, and DuP-697, an inhibitor of COX-2 (b). A summary of the SC-560-sensitive COX-1 and the DuP-697-sensitive COX-2 activities was shown in the table on the right. Enzyme activities represent means ± STDs from 6 samples. ns, nonsignificance; *, $p < 0.05$; **, $p < 0.01$; ***, $p < 0.001$; ****, $p < 0.0001$.

saline containing 0.05% Tween 20 for 1 h at room temperature to block nonspecific binding, followed by incubation of the membrane with an appropriate primary antibody. Primary antibodies used included rabbit anti-COX-1 (1:1000, #35-8100, Thermo Fisher), rabbit anti-COX-2 (1:1500, #ab179800, Abcam, Waltham, MA, USA), rabbit anti-PGES (1:1000, #702796, Thermo Fisher), and mouse anti-β-actin (1:4000, #A5441, Sigma-Aldrich, St. Louis, MO, USA) antibodies. The blot was then incubated with a second antibody, the horseradish peroxidase-conjugated goat antimouse (1:5000, #115-035-146, Jackson ImmunoResearch Laboratories,

https://doi.org/10.1021/acs.chemrestox.5c00470
Chem. Res. Toxicol. 2026, 39, 189−203

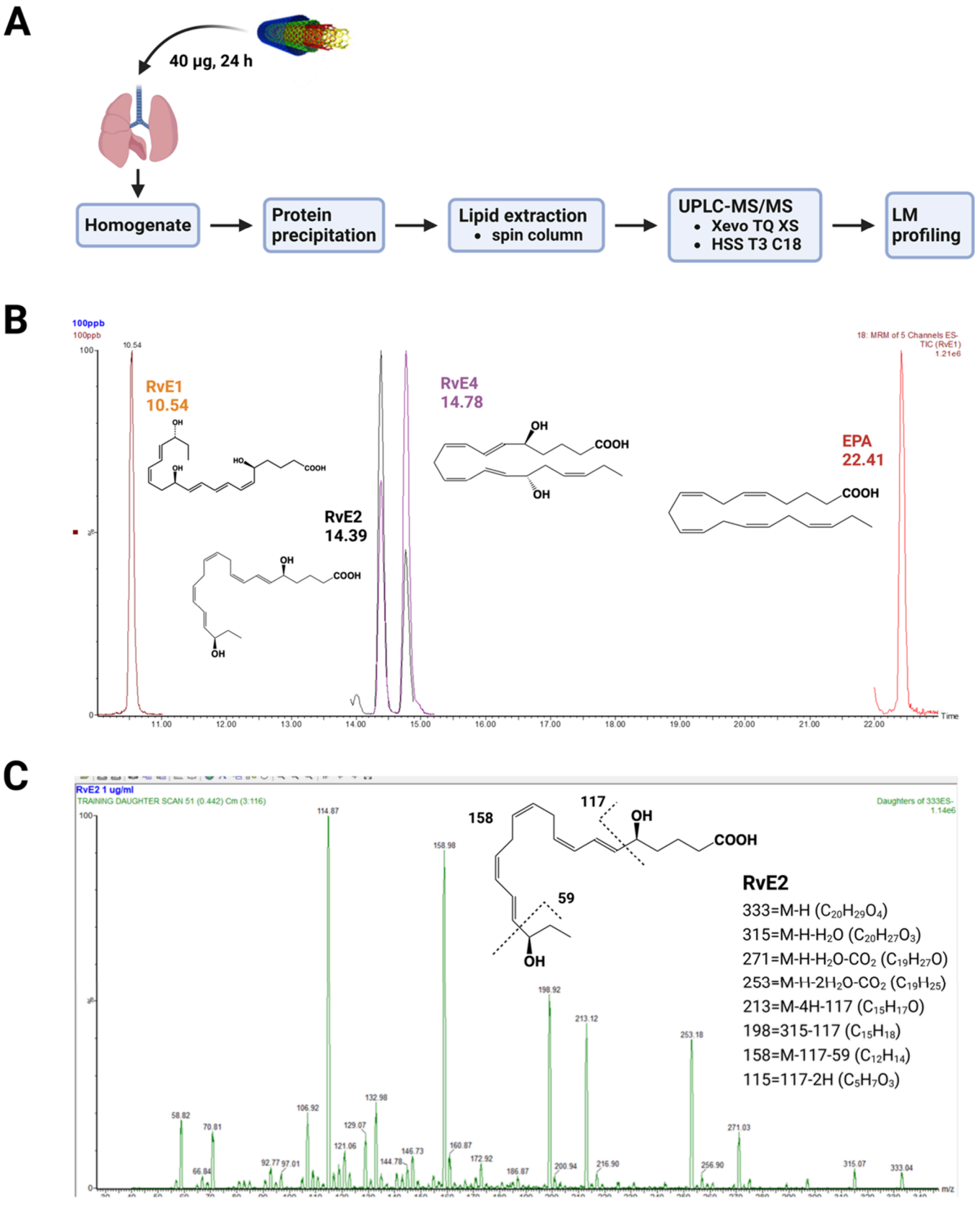

Figure 4. The UPLC-MS/MS scheme and representative UPLC chromatogram and mass spectrum. (A) A scheme for profiling LMs in mouse lung homogenates by C18 spin column solid phase extraction coupled with UPLC-MS/MS. (B) UPLC chromatogram of RvEs and EPA as an example of LM separation. The chromatogram was reconstructed from UPLC-MS/MS analysis of LMs to show the LC separation of RvE1, RvE2, RvE4, and EPA that have similar structures of the EPA subfamily. (C) Mass spectrum of RvE2 is an example of lipid ionization in mass spectrometry. Infusion of RvE2 was performed to obtain diagnostic and confirmation ion fragments of RvE2 listed in Supplemental Table 1. Major sites of fragmentation and all major ion fragments and their formulas from RvE2 were shown.

https://doi.org/10.1021/acs.chemrestox.5c00470
Chem. Res. Toxicol. 2026, 39, 189−203

West Grove, PA) or goat antirabbit IgG (1:5000, #111-035-144, Jackson ImmunoResearch Laboratories). Immunoreactive bands were visualized with enhanced chemiluminescence substrates (Thermo Fisher). Band signals were captured onto an X-ray film by exposure for 30 s, and the film was developed using a film processor (Konica Minolta, Wayne, NJ, USA). Scanned images were used to quantify band intensities using the ImageJ software (NIH), and each band was normalized to β-actin. Normalized band intensities of the MWCNT-treated group were compared to DM-treated samples and expressed as fold change.

Enzyme-Linked Immunosorbent Assay (ELISA). Proinflammatory cytokines in BALF samples were determined using ELISA. Interleukin (IL)-1β was determined using the Mouse IL-1β ELISA kit from Invitrogen (Thermo Fisher, Waltham, MA, USA), and tumor necrosis factor-α (TNF-α) was determined using the Mouse DuoSet ELISA kit from R&D Systems (Minneapolis, MN, USA), following standard procedures from the vendors. Optical densities at 450 nm were determined using the Synergy H1 microplate reader equipped with GEN5 software (Agilent Technologies).

Statistical Analysis. Dependent measures were analyzed using mixed-model one-way analyses of variance (ANOVA), with each analysis incorporating an experiment as a random factor. For the LC-MS/MS analysis, two replicate samples were averaged to yield a single value for each animal sample. Posthoc comparisons were conducted using Fisher's least significant difference test. Differences were considered significant at the following levels: ns, nonsignificance; *, $p < 0.05$; **, $p < 0.01$; ***, $p < 0.001$; and ****, $p < 0.0001$. All analyses were performed using the Statistical Analysis System (SAS, SAS Institute, Cary, NC, USA).

RESULTS

Fibrogenic MWCNTs Induced Rapid Neutrophilic Inflammation in Mouse Lungs. To analyze lipid mediators in lung inflammation and toxicity induced by high-aspect-ratio nanomaterials, we first characterized the acute inflammation in mouse lungs exposed to Mitsui-7 MWCNTs, a prototype of fibrogenic CNTs. The MWCNTs are rod-like in shape and have a high rigidity, as shown by TEM (Figure 1A-a,b). The mean length and mean width of the CNTs are 4.46 μm and 58.5 nm, respectively.

Treatment with DM did not induce notable changes in the airways and the alveolar space, whereas MWCNTs caused rapid increases in cellularity and clustering of cells, most notably at or near where MWCNTs deposit, shown as black dots under an optical microscope (Figure 1B). Immunohistochemistry staining demonstrated the clustering of Ly-6G- and Ly-6C-positive neutrophils in areas with MWCNT deposits in MWCNTs-exposed lungs (Figures 1B-b). Similarly, there was increased clustering of Mac2-positive macrophages colocalized with MWCNT deposits (Figure 1B-d). In contrast, the alveolar structures in DM-exposed lungs were well preserved, and there were no clusters of neutrophils (Figure 1B-a) or macrophages (Figures 1B-c). Quantification showed that neutrophils were increased by 25.4-fold and macrophages by 3.9-fold by MWCNTs with statistical significance (Figure 1C-a,b).

The BAL fluid was examined for inflammation and toxicity (Figure 2). MWCNTs induced high levels of secreted IL-1β and TNF-α proteins with a 10.2-fold increase for IL-1β and a 2.1-fold increase for TNF-α compared to controls (Figure 2A,B). Neutrophil infiltration in BALF was increased by 10.9-fold (Figure 2C), whereas the lactate dehydrogenase (LDH) activity, which reflects cellular damage and toxicity, was increased by 2.1-fold (Figure 2D). All changes were statistically significant (Figure 2). These findings demonstrate that a single dose of MWCNTs at 40 μg/mouse by pharyngeal aspiration caused apparent acute inflammation and toxicity in mouse lungs.

MWCNTs Induced Key Enzymes for PG Synthesis in Mouse Lungs. Next, we examined the levels of key enzymes of PG synthesis in mouse lungs with acute inflammation. Lung homogenates were prepared, and sPLA2 (Figure 3A-a) and cPLA2 (Figure 3A-b) activities were measured in the absence or presence of TEA-PC, an inhibitor of sPLA2, or pyrrophenone, an inhibitor of cPLA2. Both sPLA2 and cPLA2 activities were low but detectable in homogenates from DM-exposed lungs, and both were markedly increased in MWCNT-exposed samples. The MWCNT-induced sPLA2 activity was largely inhibited by TEA-PC and moderately decreased by pyrrophenone, showing a differential sensitivity toward the inhibitors. The MWCNT-induced cPLA2 activity was largely inhibited by pyrrophenone as expected and was also decreased by TEA-PC, showing a high sensitivity of cPLA2 to inhibition by both inhibitors.

Immunoblotting revealed that the levels of COX-2 and PGES proteins were elevated by 5.6- and 4.3-fold by MWCNTs, respectively, compared to DM, whereas the level of COX-1 was not significantly changed by the treatment (Figure 3B). The differential effect of MWCNTs on the COX enzymes was further examined by measuring COX activities in the presence of specific inhibitors. MWCNTs elevated the total COX activity by 7.8-fold (Figure 3C-a). In DM-treated samples, COX had a low activity that was significantly inhibited by SC-560, a COX-1 inhibitor but not by DuP-697, a COX-2 inhibitor, indicating a predominant role of COX-1 in the basal activity of COX in the lung (Figure 3C-b). On the other hand, the high activity of COX induced by MWCNTs was largely abolished by DuP-697 and was moderately, albeit significantly inhibited by SC-560, demonstrating COX-2 as a major COX in MWCNT-exposed lung and a switch from the COX-1-dependent to COX-2-dependent pathway for the synthesis of prostaglandins.

Development of Targeted Lipidomics of Lung LMs Using Spin Column Solid-Phase Extraction Coupled with UPLC-MS/MS. We developed a C18 spin column-based solid-phase extraction to allow the enrichment of lipid mediators from lung homogenates rapidly and efficiently. Enriched LMs were then separated and quantified through UPLC-MS/MS using a Waters ACQUITY Xevo TQ-XS UPLC-MS system. This method provided a robust and sensitive approach for the identification and quantification of LMs, including classical eicosanoids and SPMs, from a small amount of lung tissue. The overall procedure from mouse exposure to LM profiling was outlined in Figure 4A. External standards for thirty-six LMs and metabolites produced from the AA, EPA, and DHA pathways were characterized and used for identification and calibration analysis. Five deuterium-labeled LMs were used as internal standards, as they are representatives of subfamilies of LMs structurally and are available. The 41 LM analytes and their retention time, transitions, and method parameters were described in Supplemental Table 1. The cone voltage and collision energy were individually optimized for each compound. The LOD, LOQ, and recovery data for the 41 LMs were provided in Supplemental Table 2. PGH2, PGE2, and PGD2 are isobars and were separated with peak apex resolution at high concentrations. At low concentrations, their peaks partially overlapped. As expected, certain variations were observed for the recovery of the standards, underscoring the importance of

https://doi.org/10.1021/acs.chemrestox.5c00470
Chem. Res. Toxicol. 2026, 39, 189−203

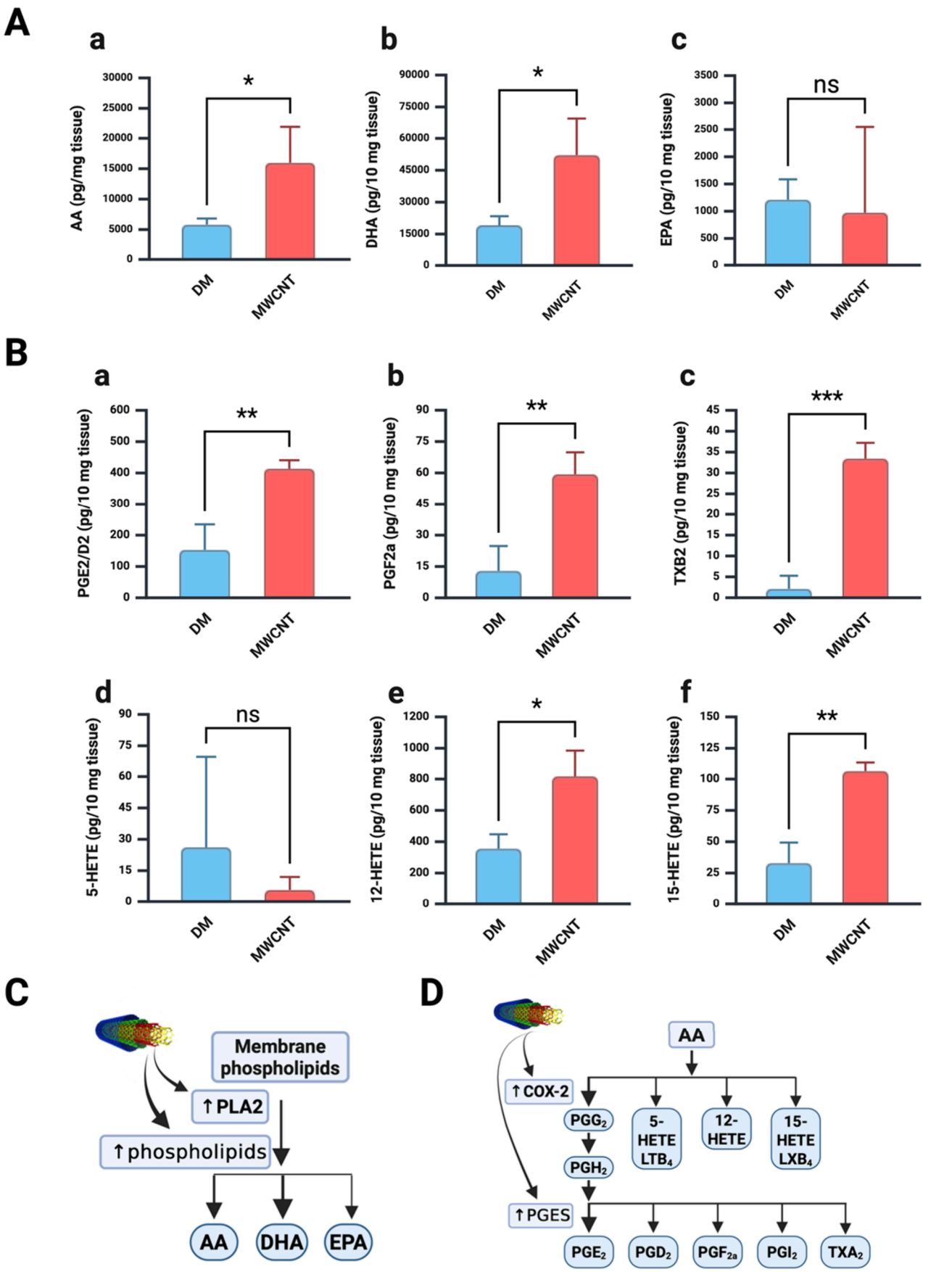

Figure 5. Elevated production of PGs in mouse lungs exposed to MWCNTS. Homogenates of lungs from mice exposed to DM or MWCNTs were analyzed to determine the levels of LMs from the PG synthesis pathway. (A) Levels of LM precursors AA (a), DHA (b), and EPA (c) in DM- or MWCNT-treated lungs are shown. (B) Levels of PGE2/D2 (a), PGF2α (b), TXB2 (c), 5-HETE (d), 12-HETE (e), and 15-HETE (f) determined

https://doi.org/10.1021/acs.chemrestox.5c00470
Chem. Res. Toxicol. 2026, 39, 189−203

Figure 5. continued

by UPLC-MS/MS are shown. (C) Illustration of the production pathway of the LM precursors affected by MWCNTs. (D) Illustration of the production pathway of PGs affected by MWCNTs. Data represent means ± STDs (n = 3). ns, nonsignificance; *, $p < 0.05$; **, $p < 0.01$; ***, $p < 0.001$.

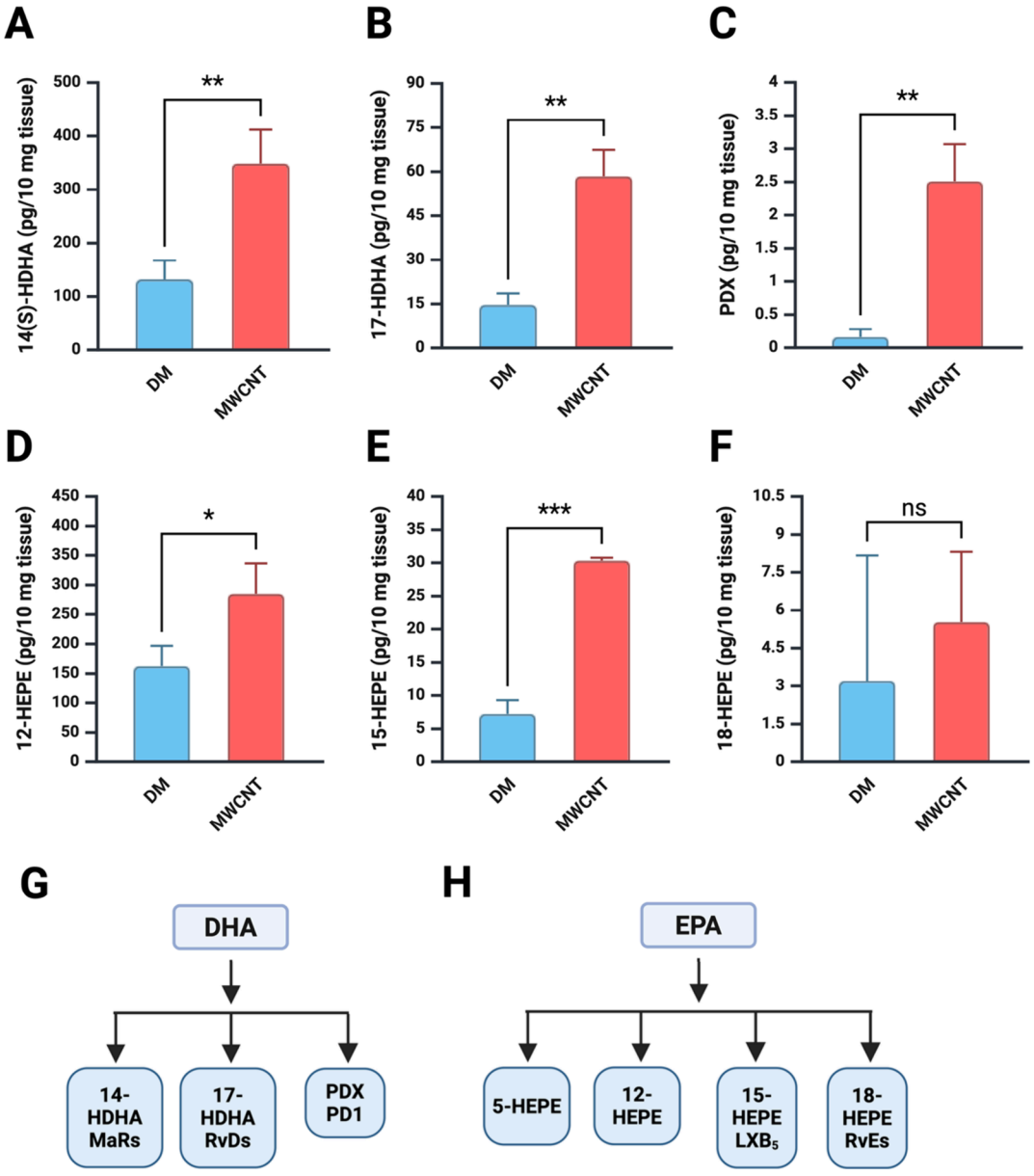

Figure 6. Production of LMs from the DHA and EPA synthesis pathways. Homogenates of lungs from mice exposed to DM or MWCNTs were analyzed to determine the levels of 14(S)-HDHA (A), 17-HDHA (B), PDX (C), 12-HEPE (D), 15-HEPE (E), and 18-HEPE (F) by UPLC-MS/MS. (G) Illustration of an increased level of synthesis of LMs from DHA. (H) Illustration of the increased synthesis of LMs from EPA induced by MWCNTs. Data represent means ± STDs (n = 3). ns, nonsignificance; *, $p < 0.05$; **, $p < 0.01$; ***, $p < 0.001$.

using internal standards for the quantification of LM analytes in lung samples.

Figure 4B shows the LC chromatogram of RvEs and EPA as an example of LM separation. The chromatogram was constructed from UPLC-MS/MS analysis of RvE1, RvE2, RvE4, and EPA that have similar structures of the EPA subfamily and for which standards are available. The LMs were well separated as individual peaks, and each has a distinctive retention time. In Figure 4C, the mass spectrum of RvE2 was shown to illustrate lipid ionization in mass spectrometry to obtain the diagnostic and confirmation ion fragments of LMs listed in Supplemental Table 1. Major fragmentation sites, all major daughter ions, and their formulas were shown (Figure 4C).

Elevated Production of PGs in Mouse Lungs Exposed to MWCNTs. Lung homogenates from mice exposed to DM or MWCNTs were used to profile the LMs. Both internal and external standards were used for the quantification of analytes. As expected, most LMs were at levels below their LOD under the basal condition, i.e., the DM-exposed group, except for AA,

https://doi.org/10.1021/acs.chemrestox.5c00470
Chem. Res. Toxicol. 2026, 39, 189−203

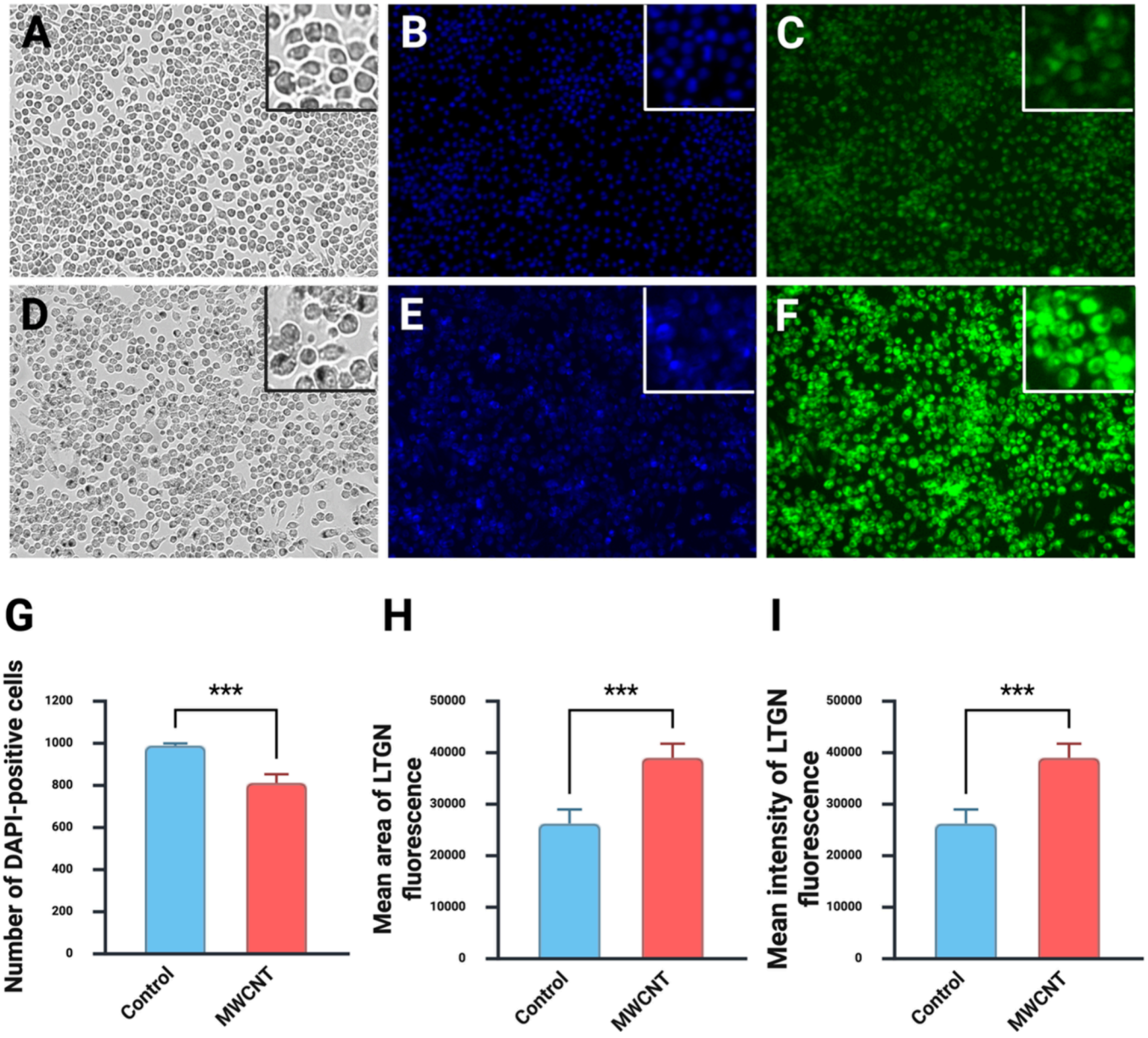

Figure 7. Effect on macrophage intracellular lipids in vitro. J774A.1 cells were cultured and treated with vehicle or MWCNTs (2 μg/mL) for 24 h followed by fluorescence staining for intracellular lipids. DAPI was used to stain the nucleus. Images were taken using the Cytation 1 Multi-Mode Reader under phase contrast (A, D), or the DAPI filter for DAPI fluorescence (B, E), or GFP filter for LipidTox Green fluorescence (C, F). Quantification of fluorescence intensity was shown in G–I. Data represent means ± STDs from 4 separate samples. Statistical significance was shown as ***, $p < 0.001$.

DHA, and EPA, which are the precursor molecules of the AA, DHA, and EPA pathways and were detected at high levels with large variations among individuals (Figure 5A). While many LMs remain at a low level or below their LODs at 24 h postexposure to a single dose of MWCNTs, there was a clear trend for elevated production of LMs and precursors from the pathway of PG synthesis. Treatment with MWCNTs significantly increased the levels of AA (Figure 5A-a) and DHA (Figure 5A-b), but not EPA (Figure 5A-c). Major prostaglandins, including PGF2α, TXB2, and PGE2 and PGD2, showed increased production induced by MWCNTs (Figure 5B-a,c). PGE2 and D2 are isobaric LMs with the same mass and similar, if not identical, ion fragments. As a result, their peaks overlap at low concentrations, and therefore, they were quantified as a combined quantity (Figure 5B-a). PGI2 and PGH2 are unstable prostaglandins under physiological conditions.[26] For this reason, PGI2 and PGH2 were not included in the quantification of the LMs. MWCNTs increased the levels of intermediate metabolites from the PG pathway, including 12-hydroxyeicosatetraenoic acid (12-HETE, Figure 5B-e) and 15-hydroxyeicosatetraenoic acid (15-HETE, Figure 5B-f), whereas the level of 5-HETE was not significantly changed (Figure 5B-d). These results demonstrate that treatment with MWCNTs elevated the level of precursors (Figure 5C) and activated the synthesis of prostaglandins and other prostanoids (Figure 5D) during acute inflammation in the lung, consistent with the rapid induction of key enzymes of PG synthesis described above.

Elevated Synthesis of SPMs from the DHA and EPA Pathways by MWCNTs. Production of SPMs is commonly

https://doi.org/10.1021/acs.chemrestox.5c00470
Chem. Res. Toxicol. 2026, 39, 189–203

associated with the resolution of inflammation. As expected, many SPMs were found to be at a low level or below their LODs in the lung under a basal condition and during the acute phase of inflammation in the lung (Figure 6A−F). Nonetheless, certain SPMs and metabolites were detected and were elevated by treatment with MWCNTs. These include 14(*S*)-hydroxydocosahexaenoic acid (14(*S*)-HDHA), 17-hydroxydocosahexaenoic acid (17-HDHA), and protectin DX (PDX or 10(*S*), 17(*S*)-dihydroxydocosahexaenoic acid) from the DHA pathway (Figure 6A−C and G) and 12-hydroxyeicosapentaenoic acid (12-HEPE) and 15-hydroxyeicosapentaenoic acid (15-HEPE) from the EPA pathway (Figure 6D, E, and H). 18-Hydroxyeicosapentaenoic acid (18-HEPE) was detected in DM-treated samples and was moderately increased by MWCNTs (Figure 6F).

MWCNTs Elevated Levels of Lipids in Macrophages In Vitro. Given the major role of macrophages in phagocytosis and clearance of MWCNTs and regulation of inflammation in mammalian lungs, we examined if MWCNTs affect lipid homeostasis in macrophages in vitro. The murine monocyte/macrophage cells J774A.1 engulf MWCNTs avidly and secrete copious amounts of inflammatory cytokines such as IL-1β upon phagocytosing MWCNTs like alveolar macrophages.[27] J774.1 macrophages were cultured and treated with MWCNTs at 2 μg/mL for 24 h followed by staining for lipids. Figure 7 showed the morphology, uptake of MWCNTs, and fluorescence staining of lipids in macrophages (Figure 7A−F). Quantification of cells and their fluorescence staining are shown in Figures 7G−I. MWCNTs were largely taken up by macrophages (Figure 7D). MWCNTs reduced the numbers of total cells, i.e., DAPI-positive cells, slightly but significantly (Figures 7G). MWCNTs significantly increased the levels of intracellular neutral lipids in macrophages, as shown by the mean area and mean intensity of the fluorescence staining (Figure 7H,I). These results revealed that MWCNTs stimulated the accumulation of lipids in macrophages in vitro, suggesting a direct effect of the phagocytosis of MWCNTs on macrophage intracellular lipid metabolism and homeostasis.

DISCUSSION

In recent years, interest has grown in understanding how inhaled nanomaterials trigger lung inflammation and how this response either resolves or progresses to chronic lesions when resolution fails.[13,16,18] Because inflammation is a common early reaction to many nanomaterials that deposit in the lungs, gaining insight into these mechanisms is essential for the toxicological evaluation and safety assessment of nanomaterials and related products. Notably, sterile inflammation caused by inhaled particles and nanoparticles differs substantially from inflammation induced by infection or tissue injury, particularly in terms of initiating stimuli, immune pathways, and persistence.[13,28] Studying nanotoxicity offers a unique opportunity to explore the host response to persistent particles and nanoparticles and their disease outcomes, which can aid in identifying biomarkers and developing targeted therapies against particle and nanoparticle toxicity.

The initiation and resolution of inflammation are tightly regulated by potent LMs including ILMs and SPMs. These LMs are produced in a temporally controlled manner and act in tissue- and cell-specific context. A major challenge in nanotoxicology is the lack of robust methods for the systematic and quantitative analysis of ILMs and SPMs. These molecules are numerous, structurally similar, and functionally complex, with intricate biosynthetic and regulatory pathways.[22] Moreover, many bioactive LMs exist in tissues at picogram levels, have short half-lives, and exhibit specific temporal profiles, consistent with their roles as paracrine and autocrine signals in the dynamic inflammatory environment. Quantitative analysis of LMs is particularly challenging in toxicological studies involving small tissue samples and multiple parameter analysis.

To address these analytical challenges in LM profiling, we developed a lipidomic workflow that integrates C18 spin column-based solid-phase extraction with UPLC-MS/MS. This optimized method enables the efficient extraction, identification, and quantification of ILMs and SPMs in mouse lungs exposed to fibrogenic MWCNTs. Our study underscores the utility of lipidomics in investigating sterile inflammation and nanotoxicity in the lung, offering insights into the molecular mechanisms underlying particle-induced immune responses. Given the complexity of lipid mediator biology and the inherent challenges in their detection discussed above, our methodology provides a new approach for future studies aiming to systematically profile lipid mediators in small tissue volumes.

We first characterized the pulmonary inflammatory response to MWCNTs to establish a suitable model for LM profiling. A single oropharyngeal dose of 40 μg/21.5 g body weight of Mitsui-7, a rod-like MWCNT, induced marked lung inflammation within 24 h. This acute response was characterized by neutrophil infiltration and the clustering of neutrophils and macrophages around deposited nanoparticles (Figure 1). MWCNT exposure significantly elevated the levels of inflammatory cytokines IL-1β and TNF-α, as well as the neutrophil count and LDH activity—a marker of lung damage—in BALF (Figure 2). These findings demonstrate that Mitsui-7 MWCNTs provoke acute lung inflammation, validating this model for further mechanistic and molecular analysis.

In view of the prominent inflammation observed and the central role of prostaglandins in the initiation and propagation of inflammatory responses, we examined the prostaglandin synthesis pathway. Our data showed significant upregulation of key enzymes involved in prostaglandin biosynthesis at both protein and activity levels (Figure 3). Specifically, sPLA2 and cPLA2 were induced and activated, facilitating the release of AA from the phospholipids. While COX-1 maintained basal cyclooxygenase activity and was not induced by MWCNTs, COX-2 was highly upregulated, accounting for elevated COX activity in exposed lungs. PGES was significantly upregulated, leading to an increased level of synthesis of PGE2 from PGH2. To the best of our knowledge, this is the first study to examine the enzymatic pathway of prostaglandin synthesis in MWCNT-induced lung inflammation and toxicity.

To quantify major ILMs and SPMs, we optimized a lipidomic method by using a C18 spin column to enable rapid and efficient enrichment of LMs from small tissue samples, such as 10 mg of lung tissue, followed by UPLC-MS/MS analysis (Figure 4). The Xevo TQ-XS Tandem Quadrupole Mass Spectrometer, coupled with the ACQUITY UPLC system and Premier HSS T3 column, provided the sensitivity and resolution needed for detection and quantification of 41 LMs at picogram levels (Figure 4 and Supplemental Tables 1 and 2). Using this method, we successfully quantified three precursor lipids (AA, DHA, and EPA), major prostanoids from the prostaglandin pathway, and selected SPMs and inter-

https://doi.org/10.1021/acs.chemrestox.5c00470
Chem. Res. Toxicol. 2026, 39, 189−203

mediates from the AA, DHA, and EPA pathways (Figures 5 and 6). AA, DHA, and EPA were detected at high levels with variations at basal conditions; and AA and DHA levels were significantly elevated following MWCNT exposure, supporting their roles as precursors for LM and SPM synthesis. In contrast, LM and SPM levels were low or undetectable in DM-treated control samples, where inflammation was minimal. MWCNT-induced inflammation led to significant increases in proinflammatory prostanoids, including PGE2, PGD2, PGF2α, TXB2, 12-HETE, and 15-HETE. Additionally, SPMs and intermediates such as 14(*S*)-HDHA, 17-HDHA, and PDX (from DHA), and 12-HEPE and 15-HEPE (from EPA), were identified. Among the prostanoids, PGE2 and PGD2 are isobaric compounds with identical masses and similar ion fragments, resulting in partial overlap of their ion peaks at low concentrations. Therefore, they were quantified together in this study. PGH2, also isobaric with PGE2 and PGD2, was successfully separated and quantified using our UPLC-MS/MS method (Supplemental Tables 1 and 2). However, due to its short half-life—like PGI2—PGH2 was not included in the tissue-level quantification.[26]

Most MWCNTs were found localized within the cytoplasm of lung macrophages (Figure 1), indicating that a majority of deposited MWCNTs were phagocytosed by these immune cells for clearance. This observation implicates macrophages as a central source of elevated ILMs and SPMs during particle-induced lung inflammation. It also suggests a direct impact of MWCNTs on lipid homeostasis within macrophages. To investigate this hypothesis, we examined the lipid accumulation in macrophages exposed to MWCNTs in vitro. At nonlethal concentrations, MWCNTs were efficiently internalized and induced a significant increase in intracellular lipid content, consistent with previous findings of lipid-laden macrophage formation in certain disease conditions.[29] These results suggest that MWCNTs may stimulate lipid catabolism or synthesis, leading to lipid accumulation. It is plausible that nanoparticle phagocytosis triggers remodeling of lysosomes and other membrane compartments, mobilizing, degrading, and synthesizing lipids—some of which may serve as precursors for ILM and SPM biosynthesis. Further studies are warranted to elucidate the mechanistic links among MWCNT phagocytosis, lysosomal dynamics, and intracellular lipid remodeling in macrophages exposed to nanomaterials.

The findings from this study allow us to propose a working model illustrating how MWCNTs disrupt lipid homeostasis and stimulate the synthesis of ILMs and SPMs (Figure 8). Among the LMs, prostanoids derived from arachidonic acid via COX pathways are rapidly produced by macrophages and other resident lung cells to orchestrate the acute phase of sterile inflammation following exposure to inhaled nanoparticles.[17,30] PGE2 promotes vasodilation, edema, and leukocyte recruitment while also modulating macrophage polarization and suppressing neutrophil activity during the resolution phase. PGD2, primarily released by mast cells, facilitates early leukocyte recruitment—especially eosinophils and basophils—and enhances vascular permeability and bronchoconstriction, contributing to acute inflammatory symptoms. PGF2α is involved in smooth muscle contraction and vasoconstriction, which may exacerbate airway narrowing and increase tissue stress during acute inflammation. TXB2, a stable metabolite of thromboxane A2, reflects platelet activation and promotes vasoconstriction and platelet aggregation, potentially amplifying tissue injury and microvascular dysfunction. Together, these prostanoids shape the intensity and duration of the acute inflammatory response, influencing whether lung tissue undergoes effective resolution or progresses toward chronic pathology. From this perspective, our study provides a new framework and analytical approach for comprehensive analysis of ILM and SPM functions and regulation in future investigations of particle- and nanoparticle-induced sterile inflammation and toxicity in the lung.

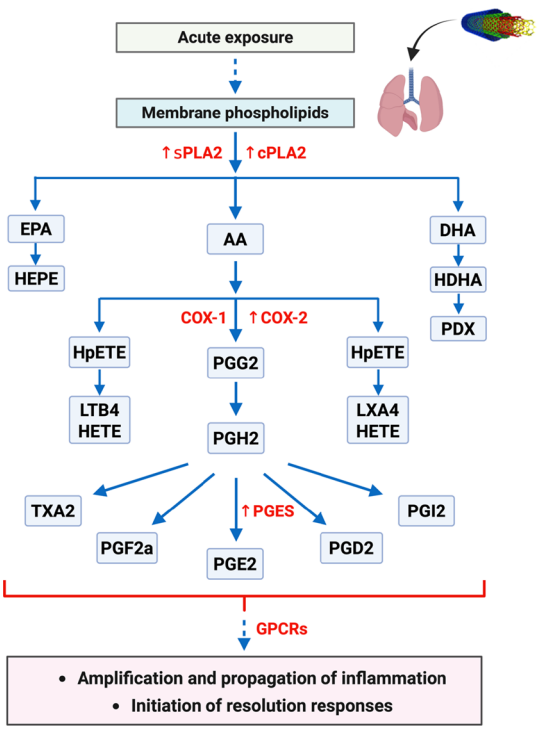

Figure 8. Schematic presentation of activation of LM production in mouse lungs by MWCNTs. LMs identified in mouse lungs by UPLC-MS/MS and induction of enzymes during MWCNT-induced acute inflammation were illustrated for pathways of LM synthesis and function. Dotted lines represent multisteps not shown in detail. LMs bind specific G-protein-coupled receptor(s) or GPCR(s) for signaling and function.

■ ASSOCIATED CONTENT

Supporting Information

The Supporting Information is available free of charge at https://pubs.acs.org/doi/10.1021/acs.chemrestox.5c00470.

Supplemental Table 1: retention time and transition ions of LM standards; and Supplemental Table 2: limit of detection (LOD), limit of quantification (LOQ), and recovery of LM standards in lung matrix (PDF)

■ AUTHOR INFORMATION

Corresponding Author

Qiang Ma − *Receptor Biology Laboratory, Toxicology and Molecular Biology Branch, Health Effects Laboratory Division, National Institute for Occupational Safety and Health, Centers for Disease Control and Prevention, Morgantown, West Virginia 26505, United States;* orcid.org/0000-0002-6379-9927; Email: qam1@cdc.gov

Authors

Ryan F. LeBouf − *Field Studies Branch, Respiratory Health Division, National Institute for Occupational Safety and*

https://doi.org/10.1021/acs.chemrestox.5c00470
Chem. Res. Toxicol. 2026, 39, 189−203

Health, Centers for Disease Control and Prevention, Morgantown, West Virginia 26505, United States

Chengetayi Cornelius Rimayi − *Field Studies Branch, Respiratory Health Division, National Institute for Occupational Safety and Health, Centers for Disease Control and Prevention, Morgantown, West Virginia 26505, United States*

Chol Seung Lim − *Receptor Biology Laboratory, Toxicology and Molecular Biology Branch, Health Effects Laboratory Division, National Institute for Occupational Safety and Health, Centers for Disease Control and Prevention, Morgantown, West Virginia 26505, United States*

Desta Fekedulegn − *Bioanalytics Branch, Health Effects Laboratory Division, National Institute for Occupational Safety and Health, Centers for Disease Control and Prevention, Morgantown, West Virginia 26505, United States*

Ju-Hyeong Park − *Field Studies Branch, Respiratory Health Division, National Institute for Occupational Safety and Health, Centers for Disease Control and Prevention, Morgantown, West Virginia 26505, United States;* orcid.org/0000-0003-4419-9341

Dale W. Porter − *Pathology and Physiology Research Branch, Health Effects Laboratory Division, National Institute for Occupational Safety and Health, Centers for Disease Control and Prevention, Morgantown, West Virginia 26505, United States;* orcid.org/0000-0002-8358-6793

Complete contact information is available at: https://pubs.acs.org/10.1021/acs.chemrestox.5c00470

Author Contributions

Q.M. and R.F.L. conceived the study; Q.M., R.F.L., C.C.R., C.S.L., J.H.P., and D.W.P. designed the study, provided reagents, and performed the study; Q.M., C.C.R., C.S.L., and R.F.L. performed UPLC-MS/MS data acquisition and analysis; D.F., Q.M., and C.S.L. performed statistical data analyses; Q.M. wrote the manuscript. All authors contributed to manuscript preparation and finalization. CRediT: **Qiang Ma** conceptualization, data curation, formal analysis, funding acquisition, investigation, methodology, project administration, resources, software, supervision, validation, visualization, writing - original draft, writing - review & editing; **Ryan F LeBouf** conceptualization, investigation, methodology, resources, software, supervision, writing - review & editing; **Chengetayi Cornelius Rimayi** formal analysis, methodology, software, validation, writing - review & editing; **Chol Seung Lim** formal analysis, funding acquisition, investigation, methodology, validation, visualization, writing - review & editing; **Desta Fekedulegn** formal analysis, methodology, software, writing - review & editing; **Ju-Hyeong Park** methodology, resources, writing - review & editing; **Dale W Porter** methodology, resources, writing - review & editing.

Funding

This work was funded by the Nanotechnology Research Center program under Grant 9390HTN (Q.M.), at the National Institute for Occupational Safety and Health, Centers for Disease Control and Prevention, USA.

Notes

The findings and conclusions in this report are those of the authors and do not necessarily represent the official position of the National Institute for Occupational Safety and Health, Centers for Disease Control and Prevention.

Mention of any company or product does not constitute endorsement by the National Institute for Occupational Safety and Health, Centers for Disease Control and Prevention.

The authors declare no competing financial interest.

REFERENCES

(1) Iijima, S. Helical microtubules of graphitic carbon. *Nature* **1991**, *354*, 56−58. Zhang, M.; Fang, S.; Zakhidov, A. A.; Lee, S. B.; Aliev, A. E.; Williams, C. D.; Atkinson, K. R.; Baughman, R. H. Strong, transparent, multifunctional carbon nanotube sheets. *Science* **2005**, *309* (5738), 1215−1219.

(2) De Volder, M. F.; Tawfick, S. H.; Baughman, R. H.; Hart, A. J. Carbon nanotubes: present and future commercial applications. *Science* **2013**, *339* (6119), 535−539. Zhang, Q.; Huang, J. Q.; Qian, W. Z.; Zhang, Y. Y.; Wei, F. The road for nanomaterials industry: a review of carbon nanotube production, post-treatment, and bulk applications for composites and energy storage. *Small* **2013**, *9* (8), 1237−1265.

(3) Hughes, K. J.; Iyer, K. A.; Bird, R. E.; Ivanov, J.; Banerjee, S.; Georges, G.; Zhou, Q. A. Review of Carbon Nanotube Research and Development: Materials and Emerging Applications. *ACS Appl. Nano Mater.* **2024**, *7*, 18695−18713.

(4) Hughes, K. J.; Cheng, J.; Iyer, K. A.; Ralhan, K.; Ganesan, M.; Hsu, C. W.; Zhan, Y.; Wang, X.; Zhu, B.; Gao, M.; et al. Unveiling Trends: Nanoscale Materials Shaping Emerging Biomedical Applications. *ACS Nano* **2024**, *18* (26), 16325−16342. Syduzzaman, M.; Saad, M. S. I.; Piam, M. F.; Talukdar, T. A.; Shod, T. T.; Pritha, N. M. Carbon nanotubes: Structure, properties and applications in the aerospace industry. *Res. Mater.* **2024**, *25*, No. 100654.

(5) Donaldson, K.; Aitken, R.; Tran, L.; Stone, V.; Duffin, R.; Forrest, G.; Alexander, A. Carbon nanotubes: a review of their properties in relation to pulmonary toxicology and workplace safety. *Toxicol. Sci.* **2006**, *92* (1), 5−22. Dong, J.; Ma, Q. Advances in mechanisms and signaling pathways of carbon nanotube toxicity. *Nanotoxicology* **2015**, *9* (5), 658−676.

(6) Porter, D. W.; Hubbs, A. F.; Mercer, R. R.; Wu, N.; Wolfarth, M. G.; Sriram, K.; Leonard, S.; Battelli, L.; Schwegler-Berry, D.; Friend, S.; et al. Mouse pulmonary dose- and time course-responses induced by exposure to multi-walled carbon nanotubes. *Toxicology* **2010**, *269* (2−3), 136−147.

(7) Dong, J.; Porter, D. W.; Batteli, L. A.; Wolfarth, M. G.; Richardson, D. L.; Ma, Q. Pathologic and molecular profiling of rapid-onset fibrosis and inflammation induced by multi-walled carbon nanotubes. *Arch. Toxicol.* **2015**, *89* (4), 621−633.

(8) Poland, C. A.; Duffin, R.; Kinloch, I.; Maynard, A.; Wallace, W. A.; Seaton, A.; Stone, V.; Brown, S.; Macnee, W.; Donaldson, K. Carbon nanotubes introduced into the abdominal cavity of mice show asbestos-like pathogenicity in a pilot study. *Nat. Nanotechnol.* **2008**, *3* (7), 423−428. Suzui, M.; Futakuchi, M.; Fukamachi, K.; Numano, T.; Abdelgied, M.; Takahashi, S.; Ohnishi, M.; Omori, T.; Tsuruoka, S.; Hirose, A.; et al. Multiwalled carbon nanotubes intratracheally instilled into the rat lung induce development of pleural malignant mesothelioma and lung tumors. *Cancer Sci.* **2016**, *107* (7), 924−935. Takagi, A.; Hirose, A.; Futakuchi, M.; Tsuda, H.; Kanno, J. Dose-dependent mesothelioma induction by intraperitoneal administration of multi-wall carbon nanotubes in p53 heterozygousmice. *Cancer Sci.* **2012**, *103* (8), 1440−1444.

(9) Dong, J.; Ma, Q. Integration of inflammation, fibrosis, and cancer induced by carbon nanotubes. *Nanotoxicology* **2019**, *13* (9), 1244−1274.

(10) Donaldson, K.; Poland, C. A.; Murphy, F. A.; MacFarlane, M.; Chernova, T.; Schinwald, A. Pulmonary toxicity of carbon nanotubes and asbestos - similarities and differences. *Adv. Drug Delivery Rev.* **2013**, *65* (15), 2078−2086.

(11) NIOSH. *Current Intelligence Bulletin 65: Occupational exposure to carbon naotubes and nanofibers*; NIOSH, 2013.

(12) Netea, M. G.; Balkwill, F.; Chonchol, M.; Cominelli, F.; Donath, M. Y.; Giamarellos-Bourboulis, E. J.; Golenbock, D.;

Gresnigt, M. S.; Heneka, M. T.; Hoffman, H. M.; et al. A guiding map for inflammation. *Nat. Immunol* **2017**, *18* (8), 826−831.
(13) Ma, Q. Polarization of Immune Cells in the Pathologic Response to Inhaled Particulates. *Front Immunol* **2020**, *11*, 1060.
(14) Dong, J.; Ma, Q. Macrophage polarization and activation at the interface of multi-walled carbon nanotube-induced pulmonary inflammation and fibrosis. *Nanotoxicology* **2018**, *12* (2), 153−168.
(15) Serhan, C. N.; Savill, J. Resolution of inflammation: the beginning programs the end. *Nat. Immunol.* **2005**, *6* (12), 1191−1197. Dong, J.; Ma, Q. Type 2 Immune Mechanisms in Carbon Nanotube-Induced Lung Fibrosis. *Front. Immunol.* **2018**, *9*, 1120.
(16) Lim, C. S.; Porter, D. W.; Orandle, M. S.; Green, B. J.; Barnes, M. A.; Croston, T. L.; Wolfarth, M. G.; Battelli, L. A.; Andrew, M. E.; Beezhold, D. H.; et al. Resolution of Pulmonary Inflammation Induced by Carbon Nanotubes and Fullerenes in Mice: Role of Macrophage Polarization. *Front Immunol* **2020**, *11*, 1186.
(17) Ricciotti, E.; FitzGerald, G. A. Prostaglandins and inflammation. *Arterioscler Thromb Vasc Biol.* **2011**, *31* (5), 986−1000.
(18) Chiang, N.; Serhan, C. N. Specialized pro-resolving mediator network: an update on production and actions. *Essays Biochem* **2020**, *64* (3), 443−462.
(19) Haeggstrom, J. Z.; Funk, C. D. Lipoxygenase and leukotriene pathways: biochemistry, biology, and roles in disease. *Chem. Rev.* **2011**, *111* (10), 5866−5898.
(20) Wallace, J. L. Prostaglandins, NSAIDs, and gastric mucosal protection: why doesn't the stomach digest itself? *Physiol Rev.* **2008**, *88* (4), 1547−1565.
(21) Serhan, C. N.; Chiang, N.; Dalli, J.; Levy, B. D. Lipid mediators in the resolution of inflammation. *Cold Spring Harb Perspect Biol.* **2015**, *7* (2), No. a016311.
(22) Dyall, S. C.; Balas, L.; Bazan, N. G.; Brenna, J. T.; Chiang, N.; da Costa Souza, F.; Dalli, J.; Durand, T.; Galano, J. M.; Lein, P. J.; et al. Polyunsaturated fatty acids and fatty acid-derived lipid mediators: Recent advances in the understanding of their biosynthesis, structures, and functions. *Prog. Lipid Res.* **2022**, *86*, No. 101165.
(23) Serhan, C. N.; Yacoubian, S.; Yang, R. Anti-inflammatory and proresolving lipid mediators. *Annu. Rev. Pathol.* **2008**, *3*, 279−312. Dalli, J.; Colas, R. A.; Walker, M. E.; Serhan, C. N. Lipid Mediator Metabolomics Via LC-MS/MS Profiling and Analysis. *Methods Mol. Biol.* **2018**, *1730*, 59−72.
(24) Lee, J. K.; Sayers, B. C.; Chun, K. S.; Lao, H. C.; Shipley-Phillips, J. K.; Bonner, J. C.; Langenbach, R. Multi-walled carbon nanotubes induce COX-2 and iNOS expression via MAP kinase-dependent and -independent mechanisms in mouse RAW264.7 macrophages. *Part Fibre Toxicol* **2012**, *9*, 14.
(25) Sayers, B. C.; Taylor, A. J.; Glista-Baker, E. E.; Shipley-Phillips, J. K.; Dackor, R. T.; Edin, M. L.; Lih, F. B.; Tomer, K. B.; Zeldin, D. C.; Langenbach, R.; et al. Role of cyclooxygenase-2 in exacerbation of allergen-induced airway remodeling by multiwalled carbon nanotubes. *Am. J. Respir. Cell Mol. Biol.* **2013**, *49* (4), 525−535.
(26) Lau, K. E.; Lui, F. *Physiology, Prostaglandin I2*; StatPearls, 2025. Wishart, D. S.; Guo, A.; Oler, E.; Wang, F.; Anjum, A.; Peters, H.; Dizon, R.; Sayeeda, Z.; Tian, S.; Lee, B. L.; et al. HMDB5.0: the Human Metabolome Database for 2022. *Nucleic Acids Res.* **2022**, *50* (D1), D622−D631.
(27) Lim, C. S.; Veltri, B.; Kashon, M.; Porter, D. W.; Ma, Q. Multi-walled carbon nanotubes induce arachidonate 5-lipoxygenase expression and enhance the polarization and function of M1 macrophages in vitro. *Nanotoxicology* **2023**, *17* (3), 249−269. Lim, C. S.; Gu, J. K.; Ma, Q. The ETS domain-containing hematopoietic transcription factor PU1 mediates the induction of arachidonate 5-lipoxygenase by multi-walled carbon nanotubes in macrophages in vitro. *Arch. Toxicol.* **2025**, *99* (2), 597−610.
(28) Ma, Q.; Lim, C. S. Molecular Activation of NLRP3 Inflammasome by Particles and Crystals: A Continuing Challenge of Immunology and Toxicology. *Annu. Rev. Pharmacol. Toxicol.* **2024**, *64*, 417−433. Huang, Y.; Jiang, W.; Zhou, R. DAMP sensing and sterile inflammation: intracellular, intercellular, and inter-organ pathways. *Nat. Rev. Immunol.* **2024**, *24* (10), 703−719.
(29) Rombouts, Y.; Neyrolles, O. The fat is in the lysosome: how Mycobacterium tuberculosis tricks macrophages into storing lipids. *J. Clin Invest* **2023**, *133* (6), No. 168366.
(30) Herschman, H. R.; Xie, W.; Reddy, S. Function and Regulation of Prostaglandin Synthase 2. In *Eicosanoids and Other Bioactive Lipids in Cancer, Inflammation, and Radiation Injury*; Honn, K. V.; Marnett, L. J.; Nigam, S.; Dennis, E. A., Eds.; Advances in Experimental Medicine and Biology, Vol. 4; Springer, 1999. Wautier, J. L.; Wautier, M. P. Pro- and Anti-Inflammatory Prostaglandins and Cytokines in Humans. *Int. J. Mol. Sci.* **2023**, *24*, 9647.

https://doi.org/10.1021/acs.chemrestox.5c00470
Chem. Res. Toxicol. 2026, 39, 189−203